

# Tests of Gravity from Imaging and Spectroscopic Surveys

Jacek Guzik,<sup>1,2,\*</sup> Bhuvnesh Jain,<sup>1,†</sup> and Masahiro Takada<sup>3,‡</sup>

<sup>1</sup>*Department of Physics and Astronomy, University of Pennsylvania, Philadelphia, PA 19104, U.S.A.*

<sup>2</sup>*Astronomical Observatory, Jagiellonian University, Orla 171, 30-244 Kraków, Poland*

<sup>3</sup>*Institute for the Physics and Mathematics of the Universe (IPMU),  
The University of Tokyo, Chiba 277-8582, Japan*

Tests of gravity on large-scales in the universe can be made using both imaging and spectroscopic surveys. The former allow for measurements of weak lensing, galaxy clustering and cross-correlations such as the ISW effect. The latter probe galaxy dynamics through redshift space distortions. We use a set of basic observables, namely lensing power spectra, galaxy-lensing and galaxy-velocity cross-spectra in multiple redshift bins (including their covariances), to estimate the ability of upcoming surveys to test gravity theories. We use a two-parameter description of gravity that allows for the Poisson equation and the ratio of metric potentials to depart from general relativity. We find that the combination of imaging and spectroscopic observables is essential in making robust tests of gravity theories. The range of scales and redshifts best probed by upcoming surveys is discussed. We also compare our parametrization to others used in the literature, in particular the  $\gamma$  parameter modification of the growth factor.

PACS numbers: 98.80.Es, 98.62.Sb

## I. INTRODUCTION

General relativity (GR) plus the Standard Model of particle physics can only account for about 4% of the energy density inferred from observations. By introducing dark matter and dark energy, which account for the remaining 96% of the total energy budget of the universe, cosmologists have been able to account for a wide range of observations, from the overall expansion of the universe to various measures of large scale structure [1].

The dark matter/dark energy scenario assumes the validity of GR at galactic and cosmological scales and introduces exotic components of matter and energy to account for observations. Since GR has not been tested independently on these scales, a natural alternative is that GR itself needs to be modified on large scales. This possibility, that modifications of the law of gravity on galactic and cosmological scales can replace dark matter and/or dark energy, has become an area of active research in recent years. Attempts have been made to modify GR with a focus on galactic [2] or cosmological scales [3, 4, 5]. The DGP model [4], in which gravity lives in a 5-dimensional space-time, can produce a late time acceleration of the universe. Adding a correction term  $f(R)$  to the Einstein-Hilbert action [3] also allows late time acceleration of the universe to be realized.

In this paper we will focus on modified gravity (MG) theories that are designed as an alternative to dark energy (DE) to produce the present day acceleration of the universe. In these models, such as DGP and  $f(R)$  models, gravity at late cosmic times and on large-scales departs from the predictions of GR. By design, successful MG models are difficult to distinguish from viable DE models using observations of the expansion history of the universe. However, in general they predict a different growth of perturbations which can be tested using observations of large-scale structure (LSS) [6, 7, 8, 9, 10, 11, 12, 13, 14, 15, 16, 17, 18, 19, 20, 21].

LSS in MG theories can be more complicated to predict, but is also richer because different observables like lensing and galaxy clustering probe independent perturbed variables. This differs from conventional DE scenarios where the linear growth factor of the density field fixes all observables on sufficiently large-scales. Theories of LSS in these modified gravity models are still in their infancy. Most studies have focused on probes of a single growth factor with one or a few observables. Recent predictions for discriminatory power of different observables could be found in [24, 34, 36, 37, 39].

We study tests of gravity that can be made with a combination of imaging and spectroscopic surveys. Our emphasis will be on model-independent constraints of MG enabled by combining different observables. Carrying out robust tests of MG in practice is challenging as in the absence of a fundamental theory, the modifications to gravity are often

---

\*Electronic address: guzikj@gmail.com

†Electronic address: bjain@physics.upenn.edu

‡Electronic address: masahiro.takada@ipmu.jp

parametrized by free functions, to be fine tuned and fixed by observations. Recently the Parametrized Post-Friedman approach has been suggested as an attempt to describe a variety of gravity theories [22].

In §II we describe the ingredients of our modeling - parametrization of the MG models (§II A), observables used for forecasting (§II B) and covariances between observables (§II C). In §III forecasts for upcoming imaging and spectroscopic surveys are presented. We conclude in §IV. The derivation of formulas for some of the covariances used in the main text are given in the Appendix A and results for alternative MG parametrization in Appendix B.

## II. METHOD

### A. Parametrization of modifications to gravity

We are concerned with sub-horizon scales that satisfy the quasi-static, Newtonian approximation. In this regime, two effective functions characterize the departure of modified gravity theories with scalar perturbations from general relativity. We neglect additional fields that are expected to play a role on small, nonlinear scales to drive the theory to GR. Scalar perturbations in a homogeneous and isotropic universe can be described in the Newtonian (longitudinal) gauge by two potentials  $\Phi(t, \mathbf{x})$  and  $\Psi(t, \mathbf{x})$  as follows [29]

$$ds^2 = - [1 + 2\Psi(t, \mathbf{x})] dt^2 + a^2(t) [1 - 2\Phi(t, \mathbf{x})] [d\chi^2 + r(\chi)^2 d\Omega^2], \quad (1)$$

where  $a(t)$  is the scale factor and  $r(\chi)$  the comoving angular-diameter distance. Throughout this paper we assume that the universe is spatially flat, so that  $r(\chi) = \chi$ . In GR, neglecting sources of the anisotropic stress in the energy-momentum tensor, the relation  $\Phi = \Psi$  holds [29]. Moreover, the curvature potential  $\Phi$  is related to the mass density distribution  $\rho(a, \mathbf{x}) = \bar{\rho}(a)\delta(a, \mathbf{x})$  through the Poisson equation, which can be altered in MG theories. We assume that the Fourier-space analogue of the Poisson equation becomes

$$-k^2\Phi(a, \mathbf{k}) = 4\pi a^2 Gg(k)\bar{\rho}\delta(a, \mathbf{k}), \quad (2)$$

where  $Gg(k)$  is the effective gravitational constant. The relation between the curvature potential  $\Phi$  and the Newtonian potential  $\Psi$  in MG theories is parametrized as

$$\eta(k) = \frac{\Phi}{\Psi}. \quad (3)$$

There are a variety of parametrization of MG in the literature; the one described above has been suggested by a number of authors [23, 37, 39]. A more general description of modified gravity models via a Parametrized-Post-Friedman approach [22] extends to the superhorizon regime, but we opt for the two free parameters described above as we restrict ourselves to the quasi-static Newtonian regime. It is expected to be a generic feature of MG that the linear growth of structure becomes scale dependent and its time evolution gets changed with respect to the GR case [22].

The simplest possibility is that the functions  $g(k)$  and  $\eta(k)$  do not depend either on time or on scale, hence we denote  $g(k) = g_0$  and  $\eta(k) = \eta_0$ . In GR both parameters are unity, which is their fiducial value throughout the paper. Other parametrization will be discussed below; in some cases a specific scale or time dependence allows for easier constraints on modified gravity parameters.

The growth of structure in a CDM dominated universe with MG is given by

$$\ddot{\delta}(a, k) + 2H(a)\dot{\delta}(a, k) - \frac{g(k)}{\eta(k)}4\pi G\bar{\rho}\delta(a, k) = 0, \quad (4)$$

where the expansion history, given by the Hubble parameter  $H = \dot{a}/a$ , will be taken to be identical to that in the standard  $\Lambda$ CDM cosmology. The growth of structure, described by the evolution of  $\delta(a, k)$  as given in Eqn. 4, depends on the ratio of  $g(k)$  and  $\eta(k)$ . The linear growth factor  $D(a) \equiv \delta(a, k)/\delta(a_i, k)$ , which describes evolution of matter density perturbations (see Eqn. (4)) relative to their initial values  $a = a_i$ , is sensitive to this ratio. The relevant growth factor for matter peculiar velocities (in fact, its divergence) relative to the density evolution is given by  $f(a) \equiv \frac{d \ln D}{d \ln a}$ .

We also consider a popular parametrization of MG which is based on the growth exponent  $\gamma$  in the growth rate function  $f(a)$  [16, 17]. For GR with a cosmological constant it can be expressed as  $f(a) = \Omega_m(a)^\gamma$ , where  $\gamma = 0.55$  and  $\Omega_m(a)$  is the total matter density parameter. For the DGP model the growth exponent is  $\gamma = 0.68$  [16]. Other parametrization are discussed in the Appendix.

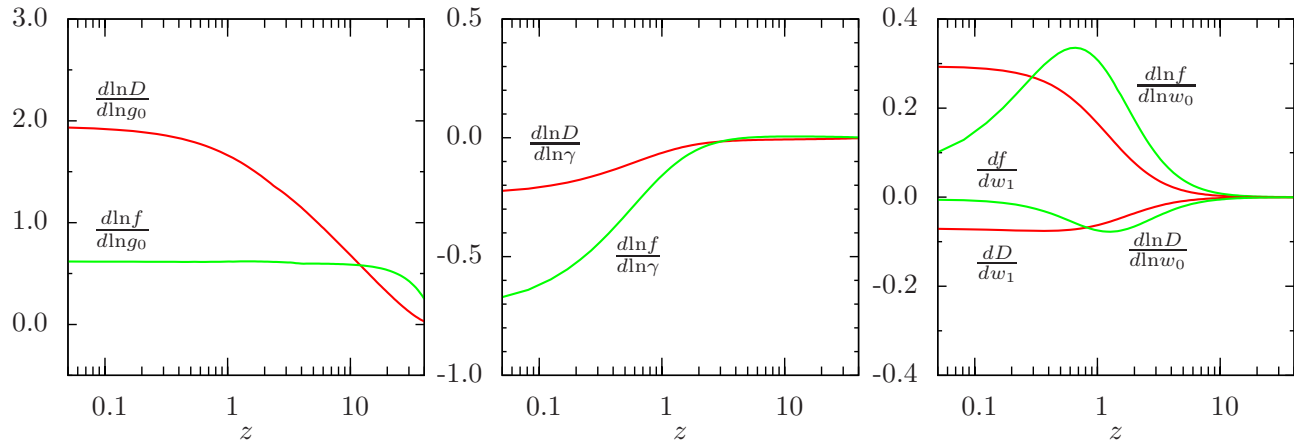


FIG. 1: Sensitivity of the growth function  $D(a)$  and the growth rate  $f(a)$  to the modified gravity parameter  $\mu_0$  (left panel), growth exponent  $\gamma$  (middle panel), and the dark energy equation of state parameters  $w_0$  and  $w_1$  (right panel) as a function of redshift.

The sensitivity of the growth factor  $D(a)$  and the growth rate function  $f(a)$  to  $\eta_0$  is shown in the Fig. 1. The effect of MG appears to be significant as for the redshift range we are interested in ( $z < 1.5$ ) the change of  $D(a)$  is  $\sim 2\%$  and  $f(a)$  is  $\sim 0.5\%$  if  $g_0$  is changed by 1% (the effect of  $\eta_0$  has the same effect but with opposite sign). If the growth exponent parametrization is employed the change in  $D(a)$  and  $f(a)$  is significantly smaller. For comparison we also show the response of  $D(a)$  and  $f(a)$  to the change of the dark energy equation of state parameters  $w_0$  and  $w_1$  defined as  $w = w_0 + w_1(1 - a)$ .

## B. Observables

We consider the signal from weak gravitational lensing together with galaxy clustering in redshift space. In metric theories of gravity the light deflection angle  $\alpha$  is given by the transverse gradient of the sum of the metric potentials:  $\alpha(\theta) = \nabla_{\perp}(\Phi + \Psi)$  (see e.g. [30]). Therefore observed shapes of galaxies and their correlations as described by weak lensing power spectra are dependent on both metric potentials. The clustering of matter is governed by the growth equation (4) which is dependent only upon the Newtonian potential. Different combinations of the information from weak lensing and redshift space galaxy clustering has been used to forecast tests of MG models [24, 34, 36].

For weak lensing we use two observables - the correlations between shapes of galaxies (cosmic shear) quantified by its power spectrum  $C_{\kappa\kappa}(l)$  and correlations between the foreground galaxy distribution and shapes of background galaxies (galaxy-galaxy lensing) described by the  $C_{g\kappa}(l)$  cross-power spectrum. We use the convergence field  $\kappa$  for simplicity as the power spectra defined below for  $\kappa$  are identical to the shear power spectra [31]. It is given by:  $\kappa(\theta) \equiv \frac{1}{2}\nabla_{\theta}^2 \alpha(\theta)$ . The relation between the convergence and the metric potentials is given by the line-of-sight projection:

$$\kappa(\theta) = \frac{1}{2} \int_0^{z_s} \frac{dz}{H(z)} \frac{r(z)r(z_s, z)}{r(z_s)} \nabla_{\theta}^2 (\Phi + \Psi), \quad (5)$$

where  $r(z)$  is the comoving angular-diameter distance between observer and a lens at redshift  $z$ . We take the sources to lie at redshift  $z_s$ .

The metric potentials are related to the mass distribution as given by Eqns. (2) and (3), so the lensing power spectra can be expressed in terms of the three-dimensional mass power spectrum  $P_{\delta\delta}(a, k)$ . In the small-sky-patch limit (we work with scales smaller than  $\sim 6^\circ$  or  $l > 30$ ), the Limber approximation [54] gives

$$C_{\kappa_i \kappa_j}(l) = \frac{9}{4} \Omega_m^2 H_0^4 \int_0^\infty \frac{dz}{H(z)} \frac{1}{a^2(z)} \left[ g(k) \frac{1 + \eta(k)}{\eta(k)} \right]^2 P_{\delta\delta}(k, z) W_L(z, z_i) W_L(z, z_j), \quad (6)$$

where the lensing weight function

$$W_L(z, z_k) = \int_{z_k} dz_k \frac{dn_b}{dz_k} \frac{r(z_k, z)}{r(z_k)}, \quad (7)$$

depends on the geometry and the redshift distribution of lensed galaxies  $dn_b/dz$ . The three-dimensional wavenumber  $k$  is given by  $k = l/r(z)$ . We use lensing tomography [53] by dividing the galaxy distribution into  $N_z$  bins in redshift. Hence, instead of one projected power spectrum we obtain  $N_z(N_z + 1)/2$  power spectra  $C_{\kappa_i \kappa_j}(l)$  that carry additional information about the growth of structure. Similarly for the galaxy-shear power spectra we have

$$C_{g_i \kappa_j}(l) = \frac{3}{2} \Omega_m H_0^2 \int_{z_i} dz_i \frac{b(z_i)}{a(z_i) r(z_i)} \frac{dn_f}{dz_i} \left[ g(k) \frac{1 + \eta(k)}{\eta(k)} \right] P_{\delta\delta}(k, z_i) W_L(z, z_j). \quad (8)$$

We assume that the distribution of galaxies  $\delta_g$  is a biased tracer of the mass distribution  $\delta$  but their relation is local and given by a bias factor  $b$  which may depend on time,  $\delta_g(z_i) = b(z_i)\delta(z_i)$ . A non-zero  $C_{g_i \kappa_j}$  is obtained when galaxies  $g_i$  are in front of the source galaxies, which requires  $i \leq j$ . We also compute the galaxy-galaxy projected power spectrum which will not be used as an observable but is required in making forecasts for MG by means of the Fisher matrix approach. It is given by

$$C_{g_i g_j}(l) = \delta_{ij} \int_{z_i} dz_i \frac{b^2(z_i)}{r^2(z_i)} H(z_i) \left[ \frac{dn_f}{dz_i} \right]^2 P_{\delta\delta}(k, z_i), \quad (9)$$

where we have assumed that galaxies in two redshift bins are not correlated with each other, a good approximation for wide enough redshift bins.

Note that the ‘observed’ power spectra differ from the spectra in Eqns. (6), (8), (9) because the effect of discrete sampling of the underlying convergence and galaxy density fields should be taken into account. It leads to shot (shape) noise terms in the case of the ‘observed’ galaxy (shear) power spectra

$$\hat{C}_{g_i g_j} = C_{g_i g_j} + \delta_{ij} / n_g^{2d}, \quad (10)$$

$$\hat{C}_{\kappa_i \kappa_j} = C_{\kappa_i \kappa_j} + \sigma_e^2 \delta_{ij} / n_g^{2d}, \quad (11)$$

$$\hat{C}_{g_i \kappa_j} = C_{g_i \kappa_j}, \quad (12)$$

where  $n_g^{2d}$  is the projected density of galaxies. The shape noise term, proportional to  $\sigma_e$ , accounts for the intrinsic ellipticities of galaxies and its value (per component) is taken to be  $0.4/\sqrt{2}$ . The cross-power spectra  $C_{g_i \kappa_j}$  are immune to the discrete sampling noise.

Modifications to GR enter the projected power spectra through the lensing-specific factor  $g(k) \frac{1 + \eta(k)}{\eta(k)}$  which is responsible for the relation between the mass distribution and the metric potentials. Moreover, the evolution of structure as expressed by growth functions  $D(a)$  and  $f(a)$  is affected by changes in gravity as a result of modifications to Eqns. (2) and (3).

In physical space, the power spectrum of the galaxy distribution  $P_{gg}(k)$  is expected to be isotropic, but in redshift space peculiar velocities distort the distribution of galaxies along the line of sight. The radial component of peculiar velocities cause the observable redshift-space power spectrum  $P_{gg}^{(s)}(k, \mu_k)$  to be ‘squashed’ along the line of sight on large scales (in the linear regime) and to produce pronounced ‘finger-of-God’ features on small scales (in the nonlinear regime) [55, 56]. The directional dependence of  $P_{gg}^{(s)}$  is given by  $\mu_k \equiv k_{\parallel}/k$ , which depends on the angle between a wave vector  $\mathbf{k}$  and the line-of-sight direction.

Although the picture is more complicated in reality (see [52] for a detailed discussion), it is a good approximation to decompose the redshift space power spectrum in terms of three isotropic power spectra relating the galaxy overdensity  $\delta_g$  and peculiar velocities  $\mathbf{v}$ : the galaxy power spectrum  $P_{gg}(k)$ , the velocity power spectrum  $P_{vv}(k)$  and the cross power spectrum  $P_{gv}(k)$  as follows [52, 55]

$$P_{gg}^{(s)}(k, \mu_k) = [P_{gg}(k) + 2\mu_k^2 P_{gv}(k) + \mu_k^4 P_{vv}(k)] F(k^2 \mu_k^2 \sigma_v^2), \quad (13)$$

where the term  $F(k^2 \mu_k^2 \sigma_v^2)$  describes non-linear velocity dispersion effects. We set  $F \approx 1$ , which is a valid on sufficiently large scales for forecasting purposes. As before, we assume that galaxies are biased tracers of mass and the bias is time-dependent but scale independent. What we refer to as the velocity is actually the velocity divergence, which is related to the mass distribution through the continuity equation in the linear regime  $\dot{\delta} + \nabla \cdot \mathbf{v}/a = 0$  (see [58]). Even if gravity is modified the continuity equation stays unchanged as long as there are no components interacting with matter.

The redshift space power spectrum in the form (13) shows a distinctive pattern in its angular dependence which is important in obtaining the component power spectra from  $P_{gg}^{(s)}$ ; it has been used to measure  $P_{gg}(k)$ ,  $P_{gv}(k)$  and

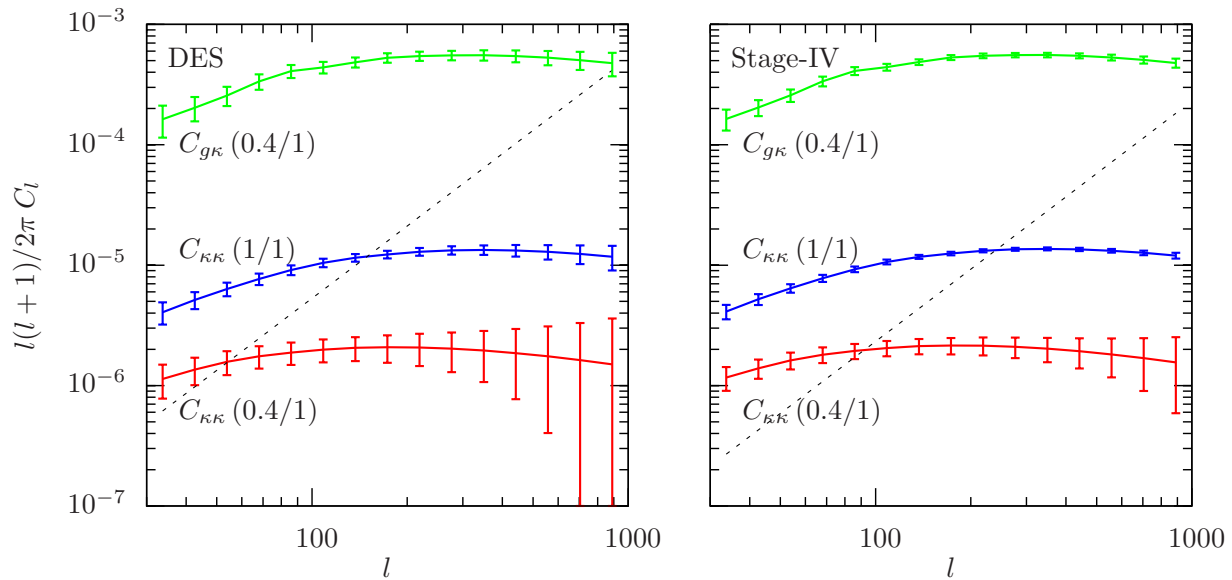


FIG. 2: Examples of the shear-shear and galaxy-shear power spectra for the DES (left panel) and a Stage-IV survey (right panel). From top: the galaxy-shear cross power spectrum  $C_{g\kappa}$  with foreground galaxies at  $z = 0.4$  and background galaxies at  $z = 1$ , the shear-shear auto power spectrum  $C_{\kappa\kappa}$ . The shape noise contribution to the auto power spectrum for  $z = 1$  is shown as well (dashed). Note that the shape noise and galaxy shot noise contribute to the variance of the power spectra.

$P_{vv}(k)$  power spectra from the 2dF and SDSS galaxy surveys [57, 59]. Moreover, this decomposition is immune to the scale dependence of both the galaxy bias and growth functions as long as the angular structure is preserved [52].

The galaxy-velocity power spectrum  $P_{gv}$  which we would like to use in constraining MG models is not a direct observable. We construct an estimator of  $P_{gv}$  band-power spectra as follows

$$\hat{P}_{gv}(k_i) = \frac{1}{N_k} \sum_{k,\mu} W_{gv}(\mu) \hat{P}_{gg}^{(s)}(k, \mu), \quad (14)$$

where the summation is carried out over modes in a spherical shell of radius  $k_i$ , and the weight function  $W_{gv}(\mu)$  is given by

$$W_{gv}(\mu) = \frac{15}{4} P_2(\mu) - \frac{135}{8} P_4(\mu), \quad (15)$$

in terms of Legendre polynomials  $P_l(\mu)$  of order  $l$  (see Appendix A for motivation of this expression). The summation in Eqn. (14) is carried out over modes contained in spherical shells in Fourier space which satisfy the following condition  $k_i - \Delta k_i/2 \leq |\mathbf{k}| \leq k_i + \Delta k_i/2$ . The volume  $V_k$  of this shell can be approximated by  $V_k = 4\pi k_i^2 \Delta k_i$ . The fundamental volume can be expressed in terms of the survey volume  $V_s$  as  $V_F = (2\pi)^3/V_s$ . The number of modes in the volume  $V_k$  is then given by  $N_k = V_k/V_F$ . We assume that the power spectrum  $\hat{P}_{gg}^{(s)}(k, \mu)$  does not vary significantly in the shell as a function of  $|\mathbf{k}|$ . We also assume that the survey is large enough that the fundamental volume is much smaller than  $V_k$ .  $\hat{P}_{gv}(k_i)$  is taken as an observable in the Fisher matrix analysis. Note that the redshift space power spectrum does not get any additional modifying factors in MG (except for the growth functions), as the continuity equation on which the relation between  $P_{gg}^{(s)}$  and  $P_{gv}$  is based remains the same.

In the present work we focus on the galaxy-velocity cross power spectrum  $P_{gv}(k)$  and the information it can deliver about the growth of structure and galaxy bias. The bias factor appears linearly in our observables, both in projected power spectra as well as in  $P_{gv}(k)$ , and is degenerate with the growth functions. However, when information in  $P_{gv}(k)$  is combined with tomographic measurements of the weak lensing signal it should allow for breaking this degeneracy [24].

### C. Fisher matrix analysis

In order to forecast the minimal attainable errors on cosmological parameters we implement the Fisher information approach [43, 44] including parameters that describe modifications to gravity. We treat as observables the following

band-power spectra, as described in §II B: shear-shear power spectra  $\hat{C}_{\kappa_i \kappa_j}(l_m)$ , galaxy-shear power spectra  $\hat{C}_{g_i \kappa_j}(l_m)$  and galaxy-velocity redshift space power spectra  $\hat{P}_{gv}(k_m)$ . The data vector of the projected spectra can be written as  $\hat{D}_\nu = \left\{ \hat{C}_{\kappa_i \kappa_j}(l_m), \hat{C}_{g_i \kappa_j}(l_m), \hat{P}_{gv}(z_i, k_n) \right\}$ , where pairs of tomography bin indices  $(i, j) : j \geq i$  with  $i, j = 1, \dots, N_z$  denote independent power spectra. Each of them is comprised of  $N_l$  band-powers. There are also  $N_z$  redshift space power spectra with  $N_k$  band-powers each. Therefore, the total number of observables in the Fisher matrix analysis is  $N_z(N_z + 1) \times N_l + N_z \times N_k$ . The projected spectra and the redshift space ones are independent so we may add their Fisher matrices or merge them into one data vector as above.

The observable power spectra depend on a set of parameters  $p_i$  whose uncertainties we aim to forecast. They are the following:  $\Omega_m$  (with  $\Omega_\Lambda$  adjusted to maintain spatial flatness), initial power spectrum slope  $n_s$ , normalization of the power spectrum at the epoch of last scattering  $\Delta_\zeta^2(k_0 = 0.002/\text{Mpc})$ , and a bias parameter in each redshift bin  $b(z_i)$ . In addition we use a two parameter  $(g_0, \eta_0)$  or one parameter  $(\gamma)$  description of departures from GR (see §II A for definitions). We do not change either the dark matter or baryon physical density when other parameters are varied to avoid adding extra information from the change of the matter power spectrum shape.

The Fisher matrix, which measures the curvature of the likelihood function in parameter space around its maximum, can be expressed for Gaussian distributed observables  $\hat{D}_\nu$  as [43]

$$F_{ij} = \sum_{\mu, \nu} \frac{\partial \hat{D}_\mu}{\partial p_i} \text{Cov}^{-1}(\hat{D}_\mu, \hat{D}_\nu) \frac{\partial \hat{D}_\nu}{\partial p_j}. \quad (16)$$

The marginalized 68%-level error on a parameter  $p_i$  is then given by  $\sigma^2(p_i) = [F^{-1}]_{ii}$ , where  $F^{-1}$  is the inverse of the Fisher matrix. In order to proceed with forecasting we need to compute the covariance matrices in Eqn. (16). We assume that the band-powers constructed from the convergence  $\kappa$  and galaxy density  $\delta_g$  are Gaussian, which restricts the validity of our analysis to relatively large scales. An analysis of non-Gaussian effects on the lensing power spectra may be found in [45].

The Gaussianity assumption allows us to express the covariance matrices of the ‘observed’ power spectra as follows

$$\text{Cov} \left[ \hat{C}_{\kappa_i \kappa_j}(l), \hat{C}_{\kappa_m \kappa_n}(l) \right] = \left[ \hat{C}_{\kappa_i \kappa_m}(l) \hat{C}_{\kappa_j \kappa_n}(l) + \hat{C}_{\kappa_i \kappa_n}(l) \hat{C}_{\kappa_j \kappa_m}(l) \right] / f_{\text{sky}} N(l), \quad (17)$$

$$\text{Cov} \left[ \hat{C}_{g_i \kappa_j}(l), \hat{C}_{g_m \kappa_n}(l) \right] = \left[ \hat{C}_{g_i g_m}(l) \hat{C}_{\kappa_j \kappa_n}(l) \delta_{im} + \hat{C}_{g_i \kappa_n}(l) \hat{C}_{g_m \kappa_j}(l) \right] / f_{\text{sky}} N(l), \quad (18)$$

$$\text{Cov} \left[ \hat{C}_{g_i \kappa_j}(l), \hat{C}_{\kappa_m \kappa_n}(l) \right] = \left[ \hat{C}_{g_i \kappa_m}(l) \hat{C}_{\kappa_j \kappa_n}(l) + \hat{C}_{g_i \kappa_n}(l) \hat{C}_{\kappa_j \kappa_m}(l) \right] / f_{\text{sky}} N(l), \quad (19)$$

where  $f_{\text{sky}}$  is fraction of the sky covered by the survey and  $N(l) = \sum_{l_{\text{min}}}^{l_{\text{max}}} (2l + 1)$  is the number of independent modes in a passband between  $l_{\text{min}}$  and  $l_{\text{max}}$ . We assume that modes in the power spectra are uncorrelated with each other.

In our analysis the binning in multipoles  $l$  is logarithmic – we assume 15 bins in the range of multipoles from  $30 < l < 1000$ . We choose this lower limit in order to be able to apply the Limber approximation when computing lensing power spectra. The upper limit is chosen to limit the nonlinear contributions to the power spectrum. Although at the high- $l$  considered there is a nonlinear enhancement to the power spectrum, we use the linear contribution as a conservative choice since both MG effects and biasing can become complex on small scales. We will show some results that include the nonlinear enhancement.

In Fig. 2 we show example shear-shear and galaxy-shear power spectra along with the relevant errors from Eqns. (17) and (18). The shape noise contribution to the observed spectra is also shown. The power spectra are flat as we take only the linear evolution of mass perturbations into account. The errors on the power spectra scale with  $f_{\text{sky}}^{-1/2}$  (see table I).

We are interested in both  $\hat{P}_{gv}(k_i)$  and its covariance  $\text{Cov}[\hat{P}_{gv}(k_i), \hat{P}_{gv}(k_j)]$ . In order to compute the covariance one could use a standard approach and express the covariance by means of the survey’s effective volume  $V_{\text{eff}}$  as  $\sigma_{\hat{P}_{gv}}^2(k_i) = 2V_{\text{eff}}^{-1} \hat{P}_{gv}^2(k_i)$  [34, 35, 61]. The effective volume accounts for the survey window function and in the sample variance limit approaches the physical survey volume  $V_s$  [34, 35]. A drawback of this formula is that it underestimates the expected noise of the estimator  $\hat{P}_{gv}(k_i)$  and does not account for the effect of discrete sampling of redshift space with mass tracers (we thank R. Scoccimarro for drawing our attention to these issues). Let us consider the covariance matrix for the galaxy-velocity band-power spectrum  $\hat{P}_{gv}(k_i)$  defined as

$$\text{Cov}[\hat{P}_{gv}(k_i), \hat{P}_{gv}(k_j)] = \langle \hat{P}_{gv}(k_i) \hat{P}_{gv}(k_j) \rangle - P_{gv}(k_i) P_{gv}(k_j). \quad (20)$$

Using the Gaussian assumption this is given by

$$\text{Cov}[\hat{P}_{gv}(k_i), \hat{P}_{gv}(k_j)] = \frac{2(2\pi)^3}{2\pi k_i^2 \Delta k_i V_s} \delta_{ij} \int_{-1}^1 \frac{d\mu}{4} W_{gv}^2(\mu) P_{gg}^{(s)}(k, \mu). \quad (21)$$

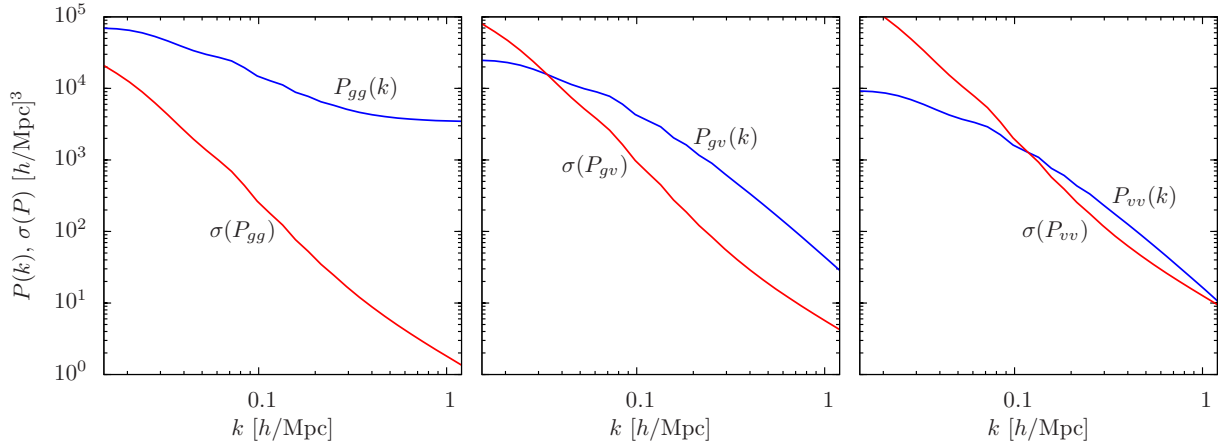


FIG. 3: The galaxy-galaxy  $P_{gg}(k)$  (left panel), galaxy-velocity  $P_{gv}(k)$  (central panel) and velocity-velocity  $P_{vv}(k)$  (right panel) power spectra at redshift  $0.5 < z < 0.7$  for the BOSS-I survey. Their expected statistical errors are shown in red. We assume 15 bins per decade in  $k$ , and do not include nonlinear effects.

Next we plug Eqn. (13) in to Eqn. (21) and integrate out the angular dependence to express the covariance matrix in terms of the component power spectra  $P_{gg}$ ,  $P_{gv}$ ,  $P_{vv}$  as follows

$$\begin{aligned} \text{Cov}[\hat{P}_{gv}(k_i), \hat{P}_{gv}(k_j)] &= \frac{2(2\pi)^3}{2\pi k_i^2 \Delta k_i V_s} \delta_{ij} \frac{105}{18304} \\ &\times \left[ 3003 \left( P_{gg}(k_i) + \frac{1}{\bar{n}_g} \right)^2 + 4420 \left( P_{gg}(k_i) + \frac{1}{\bar{n}_g} \right) P_{gv}(k_i) + 2940 P_{gv}^2(k_i) \right. \\ &\left. + 10 P_{vv}(k_i) \left\{ 147 \left( P_{gg}(k_i) + \frac{1}{\bar{n}_g} \right) + 226 P_{gv}(k_i) \right\} + \frac{24185}{51} P_{vv}^2(k_i) \right], \end{aligned} \quad (22)$$

(23)

The finite volume of the survey  $V_s$  is accounted for as well as the shot noise on small scales, which is inversely proportional to the mass tracer's density  $\bar{n}_g$ . A detailed analysis of the bias and covariance of band-power spectra estimators  $\hat{P}_{gg}$ ,  $\hat{P}_{gv}$  and  $\hat{P}_{vv}$  can be found in the Appendix. Formulas for the covariance matrices of these power spectra are presented in Eqns. (A16), (A17) and (A18).

In Fig. 3 we show galaxy and velocity power spectra,  $P_{gg}(k)$  and  $P_{vv}(k)$ , and the galaxy-velocity cross power spectrum  $P_{gv}(k)$  together with their expected errors computed as described above. The plot shows as an example the power spectra from the BOSS-I survey redshift slice centered at  $z = 0.6$  and  $\Delta z = 0.2$ . The errors on  $P_{gv}(k)$  are larger by a factor  $\sim 4$  from these on  $P_{gg}(k)$ . The good news about the cross power spectrum is that it does not suffer from the shot noise which dominates the galaxy power spectrum for  $k > 0.2 h/\text{Mpc}$ . On the other hand it is affected by sample variance; for  $k < 0.03 h/\text{Mpc}$ ,  $P_{gv}(k)$  has limited information. From Fig. 3 we see that the scale dependence of the fractional errors of  $P_{gv}(k)$  and  $P_{vv}(k)$  power spectra bears a typical u-shape with a minimum about  $k \sim 0.3 h/\text{Mpc}$ . When making error forecasts we limit our calculations to  $0.015 h/\text{Mpc} < k < 0.15 h/\text{Mpc}$  to stay within the linear regime, and use 15 logarithmic band-powers in this wavenumber range.

We compare uncertainties on redshift-space power spectra to the results of [34], whose work is closely related to ours. At the fixed scale  $k = 0.05 h/\text{Mpc}$  our method yields errors on  $P_{gg}$  which are  $\sim 3$  times smaller than presented in [34]. On the other hand errors on  $P_{vv}$  in our analysis are  $\sim 2.5$  larger than those in [34].

The total signal-to-noise ratio (S/N) for  $P_{gv}(k)$  is presented in Fig. 4 as a function of redshift. We also show the S/N for the galaxy-shear power spectra  $C_{g\kappa}$  for the DES and a Stage-IV surveys assuming that source galaxies are at fixed redshift –  $z_s = 1.1$  for DES and  $z_s = 1.9$  for the Stage-IV. As expected, the S/N is the highest when lensing galaxies are about half way to the source galaxies. The most robust constraints on MG are expected when an imaging and spectroscopic survey both have high S/N over a common redshift range. For DES and BOSS-I this occurs at redshifts between about 0.4-0.5.

It is worth noting that the S/N for  $P_{gv}(k)$  is inversely related to the bias  $b$  of the galaxy sample. A joint analysis by combining different population galaxy samples may be helpful in beating down the sample variance on large scales [46].

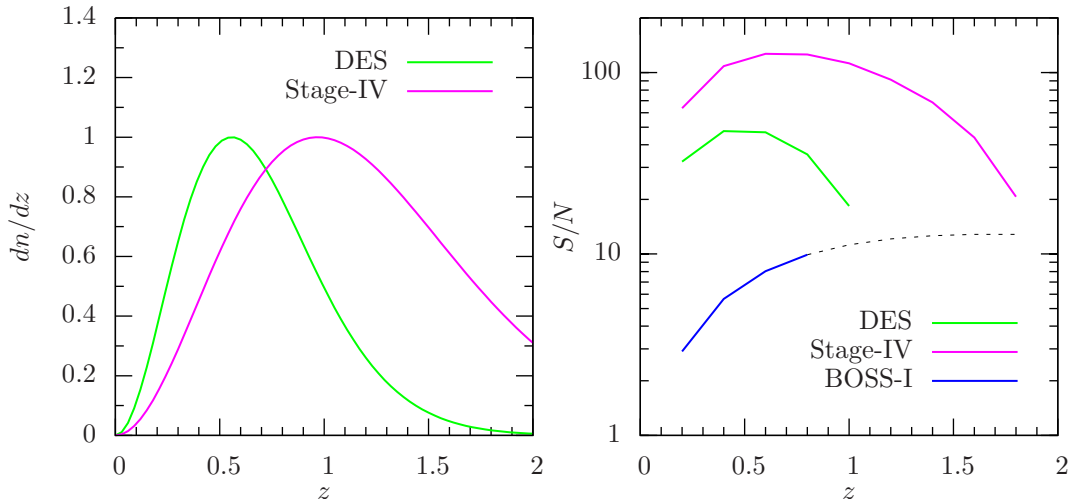


FIG. 4: Left panel: Redshift distribution of galaxies for imaging surveys specified in Table I. The distributions are normalized so that the maximum value is unity. Right panel: The total signal-to-noise ratio for the galaxy-shear power spectra  $C_{g\kappa}$  as a function of redshift of lensing galaxies. The background galaxies are located in the furthest bin –  $z = 1.2$  for DES,  $z = 2.0$  for a Stage-IV survey. The galaxy-velocity power spectrum signal-to-noise is also shown for a BOSS-I-type survey (extended to  $z = 1.9$  with the same sky coverage and galaxy density as the dotted curve).

	$f_{\text{sky}}$	$n_g^{2d}$	$z_0$	$\langle z \rangle$
DES	5000	15	0.46	0.7
Stage-IV	20000	30	0.8	1.2

TABLE I: Parameters of imaging surveys: sky coverage  $f_{\text{sky}}$  in sq. degs., galaxy surface density  $n_g^{2d}$  per sq. arcmin., the  $z_0$  parameter of the galaxy redshift distribution, and its mean  $\langle z \rangle$ .

#### D. Surveys

One of the main scientific goals of upcoming multi-color imaging surveys is to measure cosmological weak gravitational lensing. We consider two surveys of this kind: the Dark Energy Survey (DES) [48] which is expected to begin data acquisition in 2011, and a generic Stage-IV survey [42] whose example is the LSST survey [49].

The surveys are characterized by sky coverage  $f_{\text{sky}}$ , surface density of lensed galaxies  $n_g^{2d}$  and the galaxy redshift distribution. The sky coverage for the DES is taken to be 5000 sq. degs. and for the Stage-IV survey 20000 sq. degs. The redshift distribution of galaxies in the imaging surveys is assumed to have the form  $dn/dz \propto z^2 \exp[-(z/z_0)^{3/2}]$ , where the values of  $z_0$  for surveys under consideration are given in the table I and the distributions are shown in the Fig. 4.

In order to measure the redshift-space power spectrum  $P_{gg}^{(s)}$  we consider spectroscopic surveys. The Baryon Oscillation Spectroscopic Survey (BOSS) [51] will target Luminous Red Galaxies (LRG) up to redshift  $z \sim 0.7$  and will cover a quarter of the sky. It will obtain spectra of  $1.5 \times 10^6$  galaxies, which results in the number density  $\bar{n}_g = 1.1 \times 10^{-4} \text{Mpc}^{-3}$ . Based on the LRG sample from the SDSS survey one expects these objects to be biased by a factor of  $b \simeq 2$  with respect to the mass distribution. We assume that galaxies are uniformly distributed across the redshift range. In addition to the BOSS survey (called BOSS-I throughout the paper) we consider a futuristic version (dubbed BOSS-II here) with double the sky coverage compared to BOSS-I (to keep up with the sky coverage of Stage-IV survey), the same galaxy number density, and extending to redshift  $z = 1.1$ .

### III. RESULTS

We quantify constraints on modifications to gravity by combined measurements from upcoming imaging and spectroscopic surveys. Imaging surveys (see Table I) provide us with the lensing signal via  $C_{\kappa\kappa}(l)$  and  $C_{g\kappa}(l)$ . The lensing power spectra depend on the modified gravity parameters and ( $C_{g\kappa}(l)$  only) on redshift dependent galaxy bias, as given by Eqn. (8). The redshift space power spectrum  $P_{gv}(k)$  can be obtained from spectroscopic surveys. It



	$f_{\text{sky}}$	$z_{\text{min}}$	$z_{\text{max}}$	$V_s$	$\bar{n}_g$	$n_g^{2d}$
BOSS-I 10000	0.1	0.7	15.5	$1.1 \times 10^{-4}$	0.05	
BOSS-II 20000	0.1	1.1	90	$1.1 \times 10^{-4}$	0.14	

TABLE II: Parameters of the spectroscopic surveys: sky coverage  $f_{\text{sky}}$  in sq. degs., minimum and maximum redshift limits of the survey,  $z_{\text{min}}$  and  $z_{\text{max}}$ , survey comoving volume in  $\text{Gpc}^3$ , mean spatial density of galaxies  $\bar{n}_g$  per  $\text{Mpc}^3$  and their mean projected density  $n_g^{2d}$  per sq. arcmin.

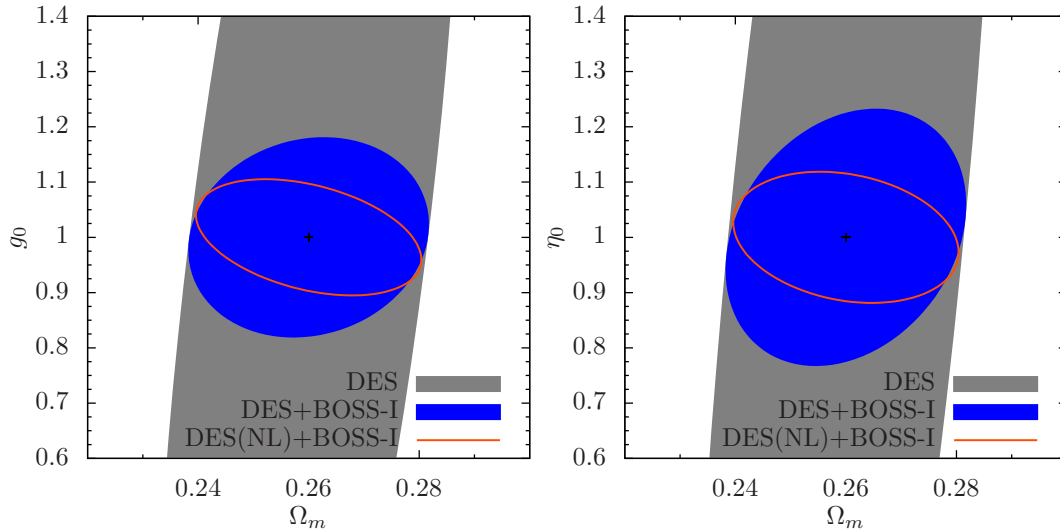


FIG. 5: Forecast constraints on the effective gravitational constant  $g_0$ , the ratio of metric potentials  $\eta_0$ , and  $\Omega_m$  for the DES imaging survey and the BOSS-I redshift survey. Forecasts based on the linear lensing power spectra (shear-shear and galaxy-shear) for DES are shown in light gray, and combined with the BOSS-I galaxy-velocity power spectrum in dark gray (blue). Light (red) inner contours show the forecasts if the nonlinear lensing power spectrum is used. Other parameters are marginalized over, and all contours show the 68% confidence level.

depends on the ratio of  $g_0$  and  $\eta_0$  and on galaxy bias.

Our fiducial cosmological model is given by  $\Omega_m = 0.26$ , the present value of the Hubble constant  $H_0 = h \times 100 \text{km/s/Mpc} = 72 \text{km/s/Mpc}$ , logarithmic slope of the initial matter power spectrum  $n = 0.96$  and its amplitude  $\Delta_\zeta^2(k_0 = 0.002/\text{Mpc}) = 2.41 \times 10^{-9}$  [25]. The redshift dependent galaxy bias is a free parameter in each redshift bin with a fiducial value  $b = 2$ , corresponding to the Luminous Red Galaxy (LRG) sample from the SDSS. Fiducial values for parameters which describe modifications to gravity are set to their values in GR:  $g_0 = \eta_0 = 1$  and  $\gamma = 0.55$ . We use statistical priors on  $\Omega_m$ ,  $\Omega_m h^2$ ,  $\Omega_b h^2$ , and the power spectrum parameters  $\Delta_\zeta^2$  and  $n$  as expected from the Cosmic Microwave Background measurements by the *Planck* satellite [28]. We also assume that the distance-redshift relation is unchanged from the standard  $\Lambda\text{CDM}$  cosmology. Therefore, MG enters the equations through the growth of structure and influences the weak lensing and redshift space power spectra, but does not affect the distance-redshift relation. Last but not least, we present uncertainties on cosmological parameters after uncertainties in the other parameters were marginalized out.

In our analysis we use tomographic measurements which require binning of the lensing and redshift-space power spectra in redshift intervals. We assume bins with width  $\Delta z = 0.2$ . Thus for the lensing spectra from the DES survey we use 6 redshift bins, while for for the Stage-IV survey we use 10 bins. For spectroscopic surveys we use 3 redshift bins for BOSS-I and 5 for BOSS-II. The projected density of spectroscopic galaxies is smaller by a factor of a few tens than for the imaging surveys, as given in tables I and II. This affects the errors on  $C_{gg}$  large but does not effect  $C_{g\kappa}$  which is one of our observables.

Our results on MG parameters constraints for the DES and BOSS-I surveys are shown in Fig. 5. If we consider weak lensing observables only (with CMB priors as described above) the one-sigma error on  $g_0$  and  $\eta_0$  is  $\sigma(g_0) = 0.94$  and  $\sigma(\eta_0) = 1.2$ . The weak constraints are due to the strong covariance between these parameters and redshift dependent bias. However, when combined with BOSS-I the constrains on  $g_0$  and  $\eta_0$  improve to  $\sigma(g_0) = 0.12$  and  $\sigma(\eta_0) = 0.15$ , as shown in the Fig. 5. Thus redshift-space clustering data enables us to beat down errors on MG parameters by about a factor of 8 (note that the constraints on  $\Omega_m$  come mainly from the CMB prior). The BOSS-I survey as presently planned will obtain redshifts for objects with  $z < 0.7$ . With the expanded redshift survey BOSS-II, the accuracy

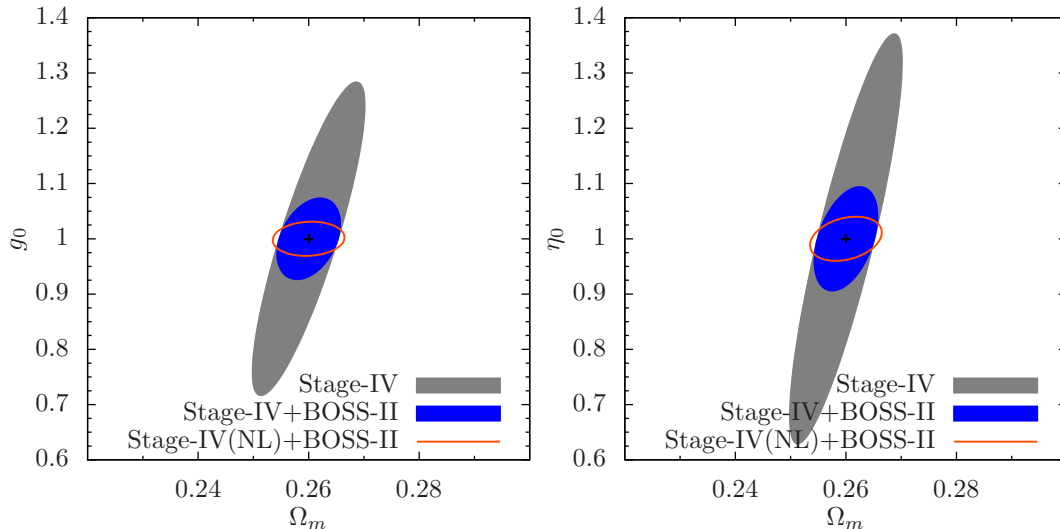


FIG. 6: Forecasts as in Fig. 5 but for a Stage-IV imaging survey and the BOSS-II spectroscopic survey.

would improve to  $\sigma(g_0) = 0.086$  and  $\sigma(\eta_0) = 0.11$ .

In order to use information on small scales from lensing one needs to model the nonlinear evolution of the matter density. Nonlinear evolution boosts the lensing signal  $C_{\kappa\kappa}(l)$  by a factor of  $\sim 4$  on scales  $l \sim 500 - 1000$ . Numerical simulations which provide nonlinear matter power spectra in MG theories are in their infancy but the first attempts are encouraging, as shown by [26] for the  $f(R)$  models and [40, 41] for the DGP model. However, there is no simple and model-independent parametrization of the nonlinear corrections to the matter power spectrum in MG models. This is due to the complexity of the evolution equations and the existence of additional fields that drive the theories to GR on small scales.

Therefore we use only the linear power spectrum up to  $l = 1000$ . This underestimates the signal-to-noise in lensing. An alternative is to use the GR-based nonlinear power spectrum, as our fiducial model is GR and small deviations from the GR may not introduce substantial deviations in the nonlinear evolution. In Fig. 5 we also show predicted uncertainties in the MG parameters if we include such a nonlinear power spectrum in the modeling of the lensing spectra. The errors on both  $g_0$  and  $\eta_0$  drop by almost a factor of 2 to  $\sigma(g_0) = 0.069$  and  $\sigma(\eta_0) = 0.078$ , respectively, compared to the linear case. This improvement is partly due to breaking the degeneracy between redshift dependent bias and MG parameters in the nonlinear regime.

We also examine Stage-IV-type surveys like LSST, which will have greater depth and sky coverage. The predictions are presented in Fig. 6. Without spectroscopic information the constraints are  $\sigma(g_0) = 0.19$  and  $\sigma(\eta_0) = 0.24$ . If we combine imaging data with the redshift-space power spectrum  $P_{gv}(k)$  from the BOSS-II survey, the constraints improve to  $\sigma(g_0) = 0.048$  and  $\sigma(\eta_0) = 0.062$ . Including nonlinear evolution in the lensing spectra leads to about a factor of two improvement.

The MG parameters are strongly correlated with each other as shown in Fig. 7. This is mostly due to the dependence of the growth factor solely on the ratio of the MG parameters. The dependence of the lensing power spectra on a different combination of MG parameters (see Eqn. (8)) is not a strong effect in practice; moreover, the change in growth can be compensated by a change in the redshift dependent galaxy bias which substantially enhances correlations. For a different MG parametrization like the one presented in the Appendix B one expects a weaker degeneracy. By combining lensing data with the redshift-space  $P_{gv}(k)$  the MG parameters are more reliably determined, as their correlation with the galaxy bias parameters is significantly reduced (see Eqns. (8) and (14)).

The importance of breaking the degeneracy between the galaxy bias and the growth of structure is highlighted in Fig. 7 by considering the dependence of uncertainties in  $g_0$  and  $\eta_0$  on the limiting projected scale  $l_{\max}$  in the lensing power spectra and the limiting physical scale  $k_{\max}$  in the  $P_{gv}(k)$  power spectrum. For DES and BOSS-I we find that these constraints are insensitive to  $l_{\max}$  if linear spectrum is used; the correlation coefficient between  $g_0$  and galaxy bias is  $r(g_0, b_i) \sim 0.8$ . The degeneracy can be broken by using the nonlinear lensing power spectra which introduces scale dependent growth, improving the constraints by a factor of  $\sim 2$  and lowering the correlation coefficient to  $r(g_0, b_i) \sim 0.5$ . Another way to beat down errors is to increase the range of  $k$ -modes in the redshift space power spectrum. However, extending the range of  $k$ -modes to  $k_{\max} > 0.15$  requires modeling nonlinear evolution and velocity dispersion effects. Throughout the paper we use linear lensing power spectra with  $l_{\max} = 1000$  and linear redshift space power spectrum with  $k_{\max} = 0.15$  h/Mpc. In this case  $r(g_0, b_i) \sim 0.8$ .

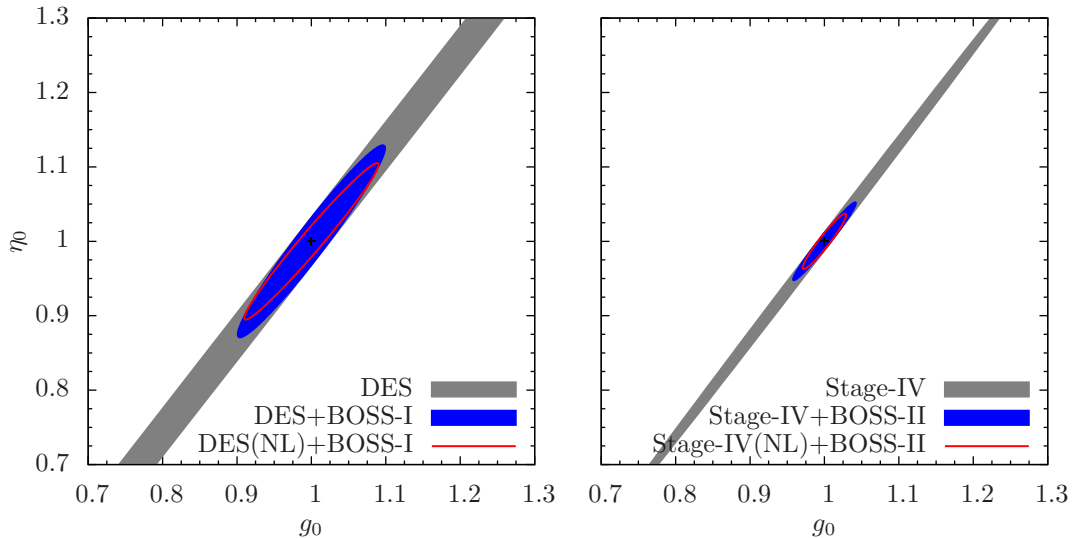


FIG. 7: Correlation between modified gravity parameters for the DES and BOSS-I surveys (left panel), and for Stage-IV surveys (right panel). The error contours are as in Fig. 5.

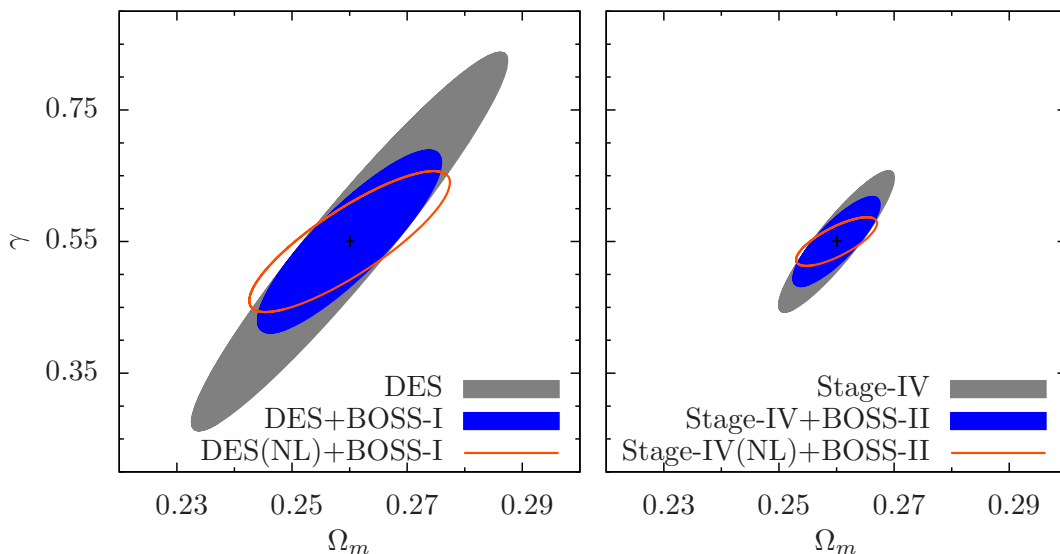


FIG. 8: Achievable errors in the growth parameter  $\gamma$  around a fiducial value  $\gamma = 0.55$ . There are shown 68% confidence level contours for survey configurations as described in Figs. 5 and 6. There are shown 68% confidence level contours as expected from the DES and Stage-IV imaging surveys (gray) and when combined with spectroscopic surveys (blue). The contour (orange) shows predictions when the nonlinear matter power spectrum is accounted for. The braneworld DGP model has  $\gamma = 0.68$ .

The bias value of a given galaxy sample is related to the S/N ratio for the redshift space power spectrum, as discussed in §II C. Lower bias implies higher signal-to-noise for  $P_{gv}(k)$ , which is counterbalanced by a lower S/N for  $C_{g\kappa}$  in the joint analysis. The net effect is that for the fiducial bias  $b = 1$  the constraints on  $g_0$  and  $\eta_0$  are virtually unchanged compared to the  $b = 2$  case which we have used in the analysis. If a less biased sample with  $b = 0.5$  is chosen, the predicted errors increase by 3%. The fiducial bias value is therefore unimportant for the purpose of this work.

We have used the  $(g_0, \eta_0)$  parametrization of MG so far. Another parametrization, based on the growth exponent  $(\gamma)$ , has been shown to be useful in distinguishing between gravity models [17]. Our results for  $\gamma$  are presented in Fig. 8. It shows that using DES lensing data we expect to constrain  $\gamma$  to  $\sigma(\gamma) = 0.19$ , while Stage-IV survey lensing data achieve  $\sigma(\gamma) = 0.07$ . When information about the redshift space power spectrum  $P_{gv}(k)$  is included the improvement is about a factor of two for DES combined with BOSS-I, and less than that for Stage IV surveys. Thus combining imaging and spectroscopic surveys is less useful for constraining  $\gamma$  than the parametrization used in the rest of the

paper (compare Fig. 7 with Figs. 5 and 6). This is not surprising, as any measure of the growth of structure constrains this one-parameter modification. While it may indeed capture the relevant physics in some MG models, in general robust constraints require tests of both the Poisson equation and the ratio of metric potentials. These require both lensing and dynamical information, as illustrated in Figs. 5 and 6.

The two models that have been extensively worked out in the literature are  $f(R)$  and DGP models; for these the ratio of potentials departs from unity by tens of percent in the quasi-static, Newtonian regime relevant to large-scale structure. The gravitational constant however is close to its value in GR if it is defined using the sum of metric potentials in the Poisson equation (rather than the usual definition, used in this paper as well, with the curvature potential) [22]. Thus  $\eta_0$  is the more sensitive parameter for testing MG if current models are used as a guide.

#### IV. CONCLUSIONS

We have used a Fisher matrix approach to test modified gravity models using imaging and spectroscopic galaxy surveys. The expansion history universe is not likely to be sufficient to test MG models as it could be mimicked by an appropriately evolving dark energy equation of state. Here we use observable consequences of the evolution of perturbations to test gravity. In particular we use weak gravitational lensing measured from multi-color imaging surveys and dynamical information from spectroscopic surveys of galaxies. Lensing is sensitive to both metric potentials, whereas dynamical effects are driven by the Newtonian potential. Combining these probes provides robust tests of gravity, which is valuable given that we currently have a very limited number of specific models that are at all plausible.

We use three simple parametrization of MG models and perform a joint analysis of shear-shear, galaxy-shear and galaxy-velocity power spectra. With a two-parameter description of modified gravity, we find that combining the three observables is essential to obtain strong constraints on gravity. We give predictions for Stage III and Stage IV surveys. We also compare the two-parameter description to the commonly used single parameter description (via the  $\gamma$  parameter), and to a scale dependent description used for braneworld models.

Our results highlight the need for imaging and spectroscopic surveys to probe the same redshift range (for the lensing mass and galaxy distribution respectively). Planned imaging surveys that reach redshifts of unity and beyond, and spectroscopic surveys that measure galaxy clustering at  $z \sim 0.2 - 0.6$  are already well suited for probing modified gravity. With a careful selection of galaxy samples to compare cross-spectra, such surveys will allow us to perform robust tests of gravity. The question of how to use small scale information requires significant work, as different modified gravity models show a variety of nonlinear effects on scales below  $\sim 10$  Mpc. It may be that models will need to be tested individually on these scales. Even so, measurements of the two parameters we have used would provide a consistency test of the GR plus a smooth dark energy scenario over a wide range of scales.

We have focused on the most common MG parametrization with the gravitational constant and the ratio of the metric potentials being free parameters. These parameters turn out to be strongly correlated with each other and with the evolving, scale independent bias for the observables we have used. With external information on bias, or by including galaxy-galaxy spectra, this degeneracy could be broken (though the bias parametrization would need to be more complex as well with the inclusion of scale dependence). Alternatively, a different, physically-motivated parametrization may be better able to capture the dependence of observables on MG, such as the one discussed in the Appendix B [32, 37]. The general properties of a useful MG parametrization, one that is able to get the most information out of a given set of observables, have been studied by [38].

Finally, in our analysis when we have included nonlinear evolution we have simply assumed it follows the predictions for GR. This provides one scenario for MG constraints; it may be optimistic as the degeneracy between MG parameters and scale independent galaxy bias gets lifted in this case. The existence of scale dependent bias on scales where nonlinear effects are important would lead to weaker constraints. On the other hand specific signatures of non-linearity would make it easier to distinguish models. Clearly more work is needed to include small scale information, realistic biasing schemes and additional observables such as galaxy power spectra, CMB lensing and the ISW effect.

#### Acknowledgments

We are grateful to Gary Bernstein, Alex Borisov, Mike Jarvis, Marcos Lima and Pengjie Zhang for many useful discussions. We especially thank Roman Scoccimarro for discussions and help with the covariance calculations. This work is supported in part by NSF grant AST-0607667. MT is supported by World Premier International Research Center Initiative (WPI Initiative), MEXT, Japan, by Grand-in-Aid for Scientific Research on Priority Area No. 467 “Probing Dark Energy through an Extremely Wide and Deep Survey with Subaru Telescope” and on young researchers (Nos. 17740129 and 20740119).

## APPENDIX A: COVARIANCE MATRICES FOR THE REDSHIFT-SPACE POWER SPECTRA

We consider distribution of mass tracers (galaxies) in the redshift space  $\delta_g^{(s)}$  and its power spectrum  $P_{gg}^{(s)}$  which is defined as [58]

$$\langle \delta_g^{(s)}(\mathbf{k}) \delta_g^{(s)}(-\mathbf{k}') \rangle = (2\pi)^3 P_{gg}^{(s)}(\mathbf{k}) \delta_D(\mathbf{k} - \mathbf{k}'), \quad (\text{A1})$$

where  $\delta_D(\mathbf{k})$  is the Dirac's delta function. In the discrete case (A1) becomes

$$\langle \delta_g^{(s)}(\mathbf{k}_i) \delta_g^{(s)}(-\mathbf{k}_j) \rangle = \frac{(2\pi)^3}{V_F} P_{gg}^{(s)}(\mathbf{k}_i) \delta_{ij}, \quad (\text{A2})$$

where discrete Fourier modes  $\delta_g^{(s)}(\mathbf{k}_i)$  have units of volume. We are interested in computing bias and covariance matrices for the galaxy-galaxy band-power spectrum  $P_{gg}(k_i)$ , galaxy-velocity  $P_{gv}(k_i)$  and velocity-velocity  $P_{vv}(k_i)$ . First, let us define estimators of these power spectra

$$\hat{P}_{XY}(k_i) = \frac{1}{N_k} \sum_{k,\mu} W_{XY}(\mu) \hat{P}_{gg}^{(s)}(k, \mu), \quad (\text{A3})$$

where  $X$  and  $Y$  stand for galaxy ( $g$ ) or velocity ( $v$ ) fields. The weight functions  $W_{XX}(\mu)$  are given by

$$W_{gg}(\mu) = P_0(\mu) - \frac{5}{2}P_2(\mu) + \frac{27}{8}P_4(\mu), \quad (\text{A4})$$

$$W_{gv}(\mu) = \frac{15}{4}P_2(\mu) - \frac{135}{8}P_4(\mu), \quad (\text{A5})$$

$$W_{vv}(\mu) = \frac{315}{8}P_4(\mu), \quad (\text{A6})$$

where  $P_l(\mu)$  is the  $l$ -th order Legendre polynomial as a function of the azimuthal angle between a wavevector  $\mathbf{k}$  and a line of sight ( $\mu_k \equiv k_{\parallel}/k$ ). The expression (A6) agrees with the one found by [60]. By ensemble averaging of (A3) one can show that weight functions (A4), (A5) and (A6) together with (A3) provide unbiased estimators for  $P_{gg}(k_i)$ ,  $P_{gv}(k_i)$  and  $P_{vv}(k_i)$ . In the continuous limit, if the fundamental volume  $V_F = (2\pi)^3/V_s$  is small compared to the total volume of the Fourier-space spherical shell  $V_k$  where averaging is carried on, we obtain

$$\langle \hat{P}_{XY}(k_i) \rangle = \frac{1}{N_k} \frac{1}{V_F} \int dk \, 2\pi k^2 \int_{-1}^1 d\mu \, W_{XY}(\mu) [P_{gg}(k_i) + 2\mu^2 P_{gv}(k_i) + \mu^4 P_{vv}(k_i)]. \quad (\text{A7})$$

Next, we use orthogonality relation for Legendre polynomials and after integration obtain

$$\langle \hat{P}_{XY}(k_i) \rangle = \frac{1}{N_k} \frac{V_k}{V_F} P_{XY}(k_i) = P_{XY}(k_i). \quad (\text{A8})$$

Therefore estimators (A3) of power spectra  $P_{gg}$ ,  $P_{gv}$  and  $P_{vv}$  are unbiased.

Now let us turn to computing covariance matrices for the introduced estimators. The formulation is general for all three band-power spectra we are interested in. The difference is in the weight functions. From the definition of the covariance matrix we have

$$\text{Cov}[\hat{P}_{XY}(k_i), \hat{P}_{XY}(k_j)] = \langle \hat{P}_{XY}(k_i) \hat{P}_{XY}(k_j) \rangle - P_{XY}(k_i) P_{XY}(k_j). \quad (\text{A9})$$

We plug Eqn. (A3) in Eqn. (A9) and obtain

$$\begin{aligned} \text{Cov}[\hat{P}_{XY}(k_i), \hat{P}_{XY}(k_j)] &+ P_{XY}(k_i) P_{XY}(k_j) \\ &= \frac{1}{N_k^2} \sum_{k,\mu} \sum_{k',\mu'} W_{XY}(\mu) W_{XY}(\mu') \langle \hat{P}_{gg}^{(s)}(k, \mu) \hat{P}_{gg}^{(s)}(k', \mu') \rangle, \end{aligned} \quad (\text{A10})$$

where averaging is over all modes in spherical shells of radii  $k$  and  $k'$  in the Fourier space. We can express the estimator of the redshift space power spectrum by means of (A2) which leads to

$$\begin{aligned} \text{Cov}[\hat{P}_{XY}(k_i), \hat{P}_{XY}(k_j)] &+ P_{XY}(k_i) P_{XY}(k_j) \\ &= \frac{1}{N_k^2} \frac{V_F^2}{(2\pi)^6} \sum_{k,\mu} \sum_{k',\mu'} W_{XY}(\mu) W_{XY}(\mu') \langle \delta_g^{(s)}(\mathbf{k}) \delta_g^{(s)}(-\mathbf{k}) \delta_g^{(s)}(\mathbf{k}') \delta_g^{(s)}(-\mathbf{k}') \rangle. \end{aligned} \quad (\text{A11})$$

Note that  $\mathbf{k}$  denotes discrete Fourier modes contained in a spherical-shell region of the Fourier space for a given band-power  $k_i$ :  $k_i - \Delta k_i/2 \leq |\mathbf{k}| \leq k_i + \Delta k_i/2$ . We assume that the  $\delta_g^{(s)}(\mathbf{k})$  is the Gaussian random field which allows to simplify (A11) considerably by applying the Wick's theorem (see e.g. [58]). We obtain

$$\begin{aligned} \text{Cov}[\hat{P}_{XY}(k_i), \hat{P}_{XY}(k_j)] + P_{XY}(k_i)P_{XY}(k_j) \\ = \frac{1}{N_k^2} \frac{V_F^2}{(2\pi)^6} \sum_{k,\mu} \sum_{k',\mu'} W_{XY}(\mu)W_{XY}(\mu') \left[ \langle \delta_g^{(s)}(\mathbf{k})\delta_g^{(s)}(-\mathbf{k}) \rangle \langle \delta_g^{(s)}(\mathbf{k}')\delta_g^{(s)}(-\mathbf{k}') \rangle \right. \\ \left. + \langle \delta_g^{(s)}(\mathbf{k})\delta_g^{(s)}(\mathbf{k}') \rangle \langle \delta_g^{(s)}(-\mathbf{k})\delta_g^{(s)}(-\mathbf{k}') \rangle + \langle \delta_g^{(s)}(\mathbf{k})\delta_g^{(s)}(-\mathbf{k}') \rangle \langle \delta_g^{(s)}(-\mathbf{k})\delta_g^{(s)}(\mathbf{k}') \rangle \right]. \end{aligned} \quad (\text{A12})$$

By applying relation (A2) we obtain

$$\begin{aligned} \text{Cov}[\hat{P}_{XY}(k_i), \hat{P}_{XY}(k_j)] + P_{XY}(k_i)P_{XY}(k_j) \\ = \frac{1}{N_k^2} \sum_{k,\mu} W_{XY}(\mu)P_{gg}^{(s)}(k,\mu) \sum_{k',\mu'} W_{XY}(\mu')P_{gg}^{(s)}(k',\mu') \\ + \frac{1}{N_k^2} \sum_{k,\mu} \sum_{k',\mu'} W_{XY}(\mu)W_{XY}(\mu') [P_{gg}^{(s)}(k,\mu)]^2 \delta_{k,k'} \delta_{\mu,-\mu'} \\ + \frac{1}{N_k^2} \sum_{k,\mu} \sum_{k',\mu'} W_{XY}(\mu)W_{XY}(\mu') [P_{gg}^{(s)}(k,\mu)]^2 \delta_{k,k'} \delta_{\mu,\mu'}. \end{aligned} \quad (\text{A13})$$

In the second and third terms we introduced Kronecker delta-type symbol  $\delta_{p,q}$  which means that only pairs of modes which wavevectors are opposite contribute to the second term and only these which wavevectors are equal contribute to the third term. These delta functions make one summation in the second and third terms drop out. Moreover, all functions are even with respect to  $\mu$ . Next, in the limit of continuous  $\mu$  we derive

$$\text{Cov}[\hat{P}_{XY}(k_i), \hat{P}_{XY}(k_j)] = \frac{2}{V_F} \frac{1}{N_k^2} \delta_{ij} \sum_k 2\pi k^2 \Delta k \int_{-1}^1 d\mu W_{XY}^2(\mu) [P_{gg}^{(s)}(k,\mu)]^2. \quad (\text{A14})$$

Finally, we obtain a general expression for the covariance of the  $P_{gg}(k_i)$ ,  $P_{gv}(k_i)$  or  $P_{vv}(k_i)$  provided validity of the decomposition (13)

$$\text{Cov}[\hat{P}_{XY}(k_i), \hat{P}_{XY}(k_j)] = \frac{2(2\pi)^3}{2\pi k_i^2 \Delta k_i V_s} \delta_{ij} \int_{-1}^1 \frac{d\mu}{4} W_{XY}^2(\mu) P_{gg}^{(s)}(k,\mu). \quad (\text{A15})$$

By means of the relation (A15) it is straightforward to obtain desired expressions for the  $\hat{P}_{gg}(k_i)$ ,  $\hat{P}_{gv}(k_i)$  and  $\hat{P}_{vv}(k_i)$  band-power-spectra covariance matrices which are presented below. Notice that we included the effect of discrete sampling of the mass tracer distribution by including the shot noise term  $1/\bar{n}_g$ .

$$\begin{aligned}
\text{Cov}[\hat{P}_{gg}(k_i), \hat{P}_{gg}(k_j)] &= \frac{2(2\pi)^3}{2\pi k_i^2 \Delta k_i V_s} \delta_{ij} \frac{75}{128128} \\
&\times \left[ 3003 \left( P_{gg}(k_i) + \frac{1}{\bar{n}_g} \right)^2 + 1092 \left( P_{gg}(k_i) + \frac{1}{\bar{n}_g} \right) P_{gv}(k_i) + \frac{1652}{3} P_{gv}^2(k_i) \right. \\
&+ \left. \frac{2}{15} P_{vv}(k_i) \left\{ 2065 \left( P_{gg}(k_i) + \frac{1}{\bar{n}_g} \right) + 3126 P_{gv}(k_i) \right\} + \frac{1491}{17} P_{vv}^2(k_i) \right], \quad (\text{A16})
\end{aligned}$$

$$\begin{aligned}
\text{Cov}[\hat{P}_{gv}(k_i), \hat{P}_{gv}(k_j)] &= \frac{2(2\pi)^3}{2\pi k_i^2 \Delta k_i V_s} \delta_{ij} \frac{105}{18304} \\
&\times \left[ 3003 \left( P_{gg}(k_i) + \frac{1}{\bar{n}_g} \right)^2 + 4420 \left( P_{gg}(k_i) + \frac{1}{\bar{n}_g} \right) P_{gv}(k_i) + 2940 P_{gv}^2(k_i) \right. \\
&+ \left. 10 P_{vv}(k_i) \left\{ 147 \left( P_{gg}(k_i) + \frac{1}{\bar{n}_g} \right) + 226 P_{gv}(k_i) \right\} + \frac{24185}{51} P_{vv}^2(k_i) \right], \quad (\text{A17})
\end{aligned}$$

$$\begin{aligned}
\text{Cov}[\hat{P}_{vv}(k_i), \hat{P}_{vv}(k_j)] &= \frac{2(2\pi)^3}{2\pi k_i^2 \Delta k_i V_s} \delta_{ij} \frac{44100}{1537536} \\
&\times \left[ 3003 \left( P_{gg}(k_i) + \frac{1}{\bar{n}_g} \right)^2 + 1092 \left( P_{gg}(k_i) + \frac{1}{\bar{n}_g} \right) P_{gv}(k_i) + \frac{23148}{5} P_{gv}^2(k_i) \right. \\
&+ \left. \frac{2}{5} P_{vv}(k_i) \left\{ 5787 \left( P_{gg}(k_i) + \frac{1}{\bar{n}_g} \right) + 9810 P_{gv}(k_i) \right\} + \frac{14931}{17} P_{vv}^2(k_i) \right]. \quad (\text{A18})
\end{aligned}$$

## APPENDIX B: ALTERNATIVE PARAMETRIZATION OF MODIFIED GRAVITY

A useful modification to GR was proposed by [32], which seeks to describe changes in the potential-density relationship on large scales while leaving small scales unchanged from GR. The modification is expressed in the form of a power series in  $aH/k$ , which is the ratio of the proper scale of perturbations  $a/k$  to the horizon size  $1/H$ . The Fourier-space analogue of the Poisson equation is assumed to be modified as follows

$$-k^2 \Phi(a, \mathbf{k}) = 4\pi a^2 G g(k) \bar{\rho} \delta(a, \mathbf{k}), \quad (\text{B1})$$

where  $g(k) \equiv g_0(a) + g_1(a) \frac{aH}{k}$ . The relation (B1) converges to GR when  $g_0 = 1$  and for scales much smaller than the horizon size, i.e.  $aH/k \gg 1$ . Note that we consider only the first two elements of the power series. The linear term in the expansion (B1) is characteristic for brane-world inspired models like DGP. The linear term is absent in scalar-tensor models including  $f(R)$  models, where the first non-zero higher order term is quadratic in  $aH/k$ . For a thorough discussion of the parametrization and specific examples in different alternative gravity models see [32].

Similar to the curvature potential  $\Phi$ , the Newtonian potential can be modified as [32]

$$-k^2 \Psi(a, \mathbf{k}) = 4\pi a^2 G \mu(k) \bar{\rho} \delta(a, \mathbf{k}), \quad (\text{B2})$$

where  $\mu(k) \equiv \mu_0(a) + \mu_1(a) \frac{aH}{k}$ . In GR  $g_0 = \mu_0 = 1$  and the scale dependence of both potentials vanishes. Thus, we parametrize the departure from GR using 4 parameters  $g_0, g_1, \mu_0$  and  $\mu_1$ . They are used in the Fisher matrix analysis with fiducial values are  $g_0 = \mu_0 = 1$  and  $g_1 = \mu_1 = 0$ . This type of modification is supported by the fact that the growth of structures is sourced by the Newtonian potential  $\Psi$ , so that  $\mu_0$  and  $\mu_1$  contain information about the effect of MG on the observed matter distribution. The growth equation takes the form [23]

$$\ddot{\delta}(a, k) + 2H(a) \dot{\delta}(a, k) + \mu(k) \frac{k^2}{a^2} \Phi(a, k) = 0. \quad (\text{B3})$$

The results for MG parameters with Stage-IV and BOSS-II surveys are shown in Fig. 9. The imaging Stage-IV survey (with the usual CMB prior) could constrain the scale-independent part of the effective gravitational constants as  $\sigma(g_0) = 0.22$  and  $\sigma(\mu_0) = 0.075$  (about a factor of 4 smaller than those achievable with DES.) If we add information from BOSS-II spectroscopic survey we obtain  $\sigma(g_0) = 0.050$  and  $\sigma(\mu_0) = 0.018$  (about 2.5 times smaller than for DES and BOSS-I.)

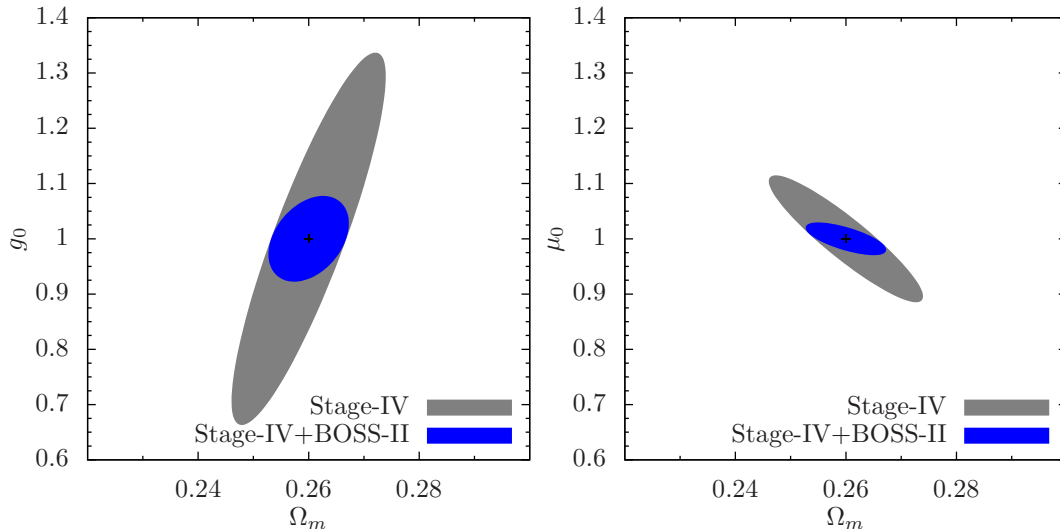


FIG. 9: Achievable uncertainty on modified gravity parameters  $g_0$ ,  $\mu_0$  and matter density  $\Omega_m$  for the future configuration of the Stage-IV imaging survey and the BOSS-II galaxy redshift survey. Predictions for the Stage-IV survey only are shown in gray, for the Stage-IV and BOSS-II combined – in blue. There are shown 68% confidence level contours. The dependence on the other parameters is marginalized out.

In Fig. 10 we present joint constraints on the scale independent and dependent terms in the modification. The uncertainties on the scale dependent terms are much larger (compared to the constant terms):  $\sigma(g_1) = 3.52$  and  $\sigma(\mu_1) = 1.39$ . The weak constraints on the scale dependent terms relates to the fact that this dependence is important on large scales approaching the horizon, where the signal-to-noise is small. The integrated Sachs-Wolfe effect would be more promising to test for modifications on the largest scales.

On the other hand, even constraining the scale independent modification lets us distinguish a class of brane-world models like DGP gravity from the standard LCDM one. The values of parameters under examination for the DGP model are  $g_0 = 1.25$ ,  $g_1 = 0.5$ ,  $\mu_0 = 0.75$ ,  $\mu_1 = 0.5$  at  $z \sim 0.2$  (and closer to GR values for higher redshifts [32]). Thus the DGP model is several  $\sigma$  away from the GR (see [62] for current constraints on DGP). The differences in the growth history in these two gravity models helps discriminate them ( $\mu_0$  is the most tightly constrained parameter).

We have also explored time evolving parametrization of  $g$  and  $\eta$ . With additional parameters, constraints generally get weaker, but if one chooses a specific fiducial time evolution (such as linear or quadratic in  $a$ ) it can become easier to test MG models. We leave a detailed exploration of time and scale dependence for future work. See [38] for a recent study using principal components in the scale and time dependence.

- 
- [1] D. N. Spergel et al. (WMAP), *Astrophys. J. Suppl. Ser.* **170**, 377 (2007); M. Tegmark et al. (SDSS), *Phys. Rev. D* **74**, 123507 (2006); A. G. Riess et al., *Astrophys. J.* **659**, 98 (2007)
  - [2] M. Milgrom, *Astrophys. J.* **207**, 371 (1983); J. D. Bekenstein, *Phys. Rev. D* **70**, 083509 (2004)
  - [3] S. M. Carroll, V. Duvvuri, M. Trodden, and M. S. Turner, *Phys. Rev. D* **70**, 043528 (2004); S. M. Carroll, A. De Felice, V. Duvvuri, D. A. Easson, M. Trodden, and M. S. Turner, *Phys. Rev. D* **71**, 063513 (2005); S. Nojiri and S. D. Odintsov, *J. Phys. A* **40**, 6725 (2007)
  - [4] G. Dvali, G. Gabadadze, and M. Porrati, *Phys. Lett. B* **485**, 208 (2000); C. Deffayet, *Phys. Lett. B* **502**, 199 (2001)
  - [5] V. Sahni, Y. Shtanov, and A. Viznyuk, *J. Cosmol. Astropart. Phys.* **12**, 5 (2005)
  - [6] M. White and C.S. Kochanek, *Astrophys. J.* **560**, 539 (2001); A. Shirata, T. Shiromizu, N. Yoshida, and Y. Suto, *Phys. Rev. D* **71**, 064030 (2005); C. Sealfon, L. Verde, and R. Jimenez, *Phys. Rev. D* **71**, 083004 (2005); A. Shirata, Y. Suto, C. Hikage, T. Shiromizu, and N. Yoshida, *Phys. Rev. D* **76**, 044026 (2007)
  - [7] C. Skordis, D. F. Mota, P. G. Ferreira, and C. Boehm *Phys. Rev. Lett.* **96**, 011301 (2006); C. Skordis, *Phys. Rev. D* **74**, 103513 (2006)
  - [8] S. Dodelson and M. Liguori, *Phys. Rev. Lett.* **97**, 231301 (2006)
  - [9] A. Lue, R. Scoccimarro, and G. Starkman, *Phys. Rev. D* **69**, 124015 (2004)
  - [10] L. Knox, Y.-S. Song, and J.A. Tyson, *Phys. Rev. D* **74**, 023512 (2005); M. Ishak, A. Upadhye, and D. N. Spergel, *Phys. Rev. D* **74**, 043513 (2006)
  - [11] K. Koyama and R. Maartens, *J. Cosmol. Astropart. Phys.* **1**, 16 (2006)



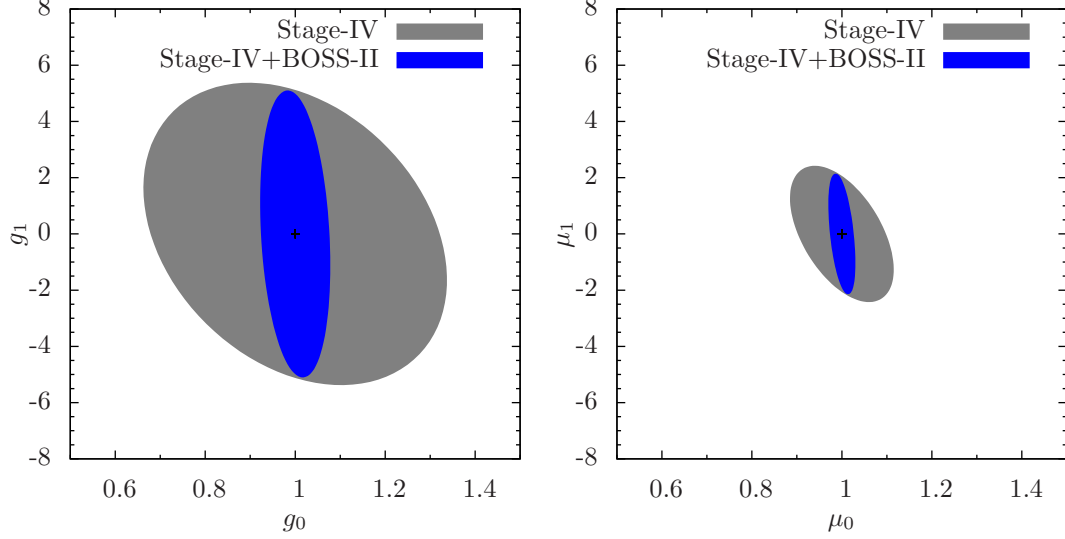


FIG. 10: Uncertainty in modified gravity parameters  $g_1$ ,  $\mu_1$  which describe scale dependence of the growth of structure. There are shown 68% confidence level contours for the Stage-IV alone and combined with BOSS-II. Note a lack of constrains on the scale dependence of the modified gravity models for the assumed parametrization.

- [12] T. Koivisto and H. Kurki-Suonio, *Class. Quant. Grav.* **23**, 2355 (2006); T. Koivisto, *Phys. Rev. D* **73**, 083517 (2006); B. Li and M.-C. Chu *Phys. Rev. D* **74**, 104010 (2006); B. Li and J. Barrow, *Phys. Rev. D* **75**, 084010 (2007)
- [13] Y. Song, W. Hu, and I. Sawicki, *Phys. Rev. D* **75**, 044004 (2006)
- [14] P. Zhang, *Phys. Rev. D* **73**, 123504 (2006)
- [15] R. Bean, D. Bernat, L. Pogosian, A. Silvestri, and M. Trodden, *Phys. Rev. D* **75**, 064020 (2007)
- [16] E. V. Linder, *Phys. Rev. D* **72**, 043529 (2005)
- [17] D. Huterer and E. V. Linder, *Phys. Rev. D* **75**, 023519 (2007)
- [18] J.-P. Uzan, *Gen. Relativ. Gravit.* **39**, 307 (2006)
- [19] R. Caldwell, A. Cooray, and A. Melchiorri, *Phys. Rev. D* **76**, 023507 (2007)
- [20] L. Amendola, M. Kunz, and D. Sapone, *J. Cosmol. Astropart. Phys.* **4**, 13 (2008)
- [21] H. Stabenau and B. Jain, *Phys. Rev. D* **74**, 084007 (2006)
- [22] W. Hu and I. Sawicki, *Phys. Rev. D* **76**, 104043 (2007)
- [23] B. Jain and P. Zhang, *Phys. Rev. D* **78**, 063503 (2008)
- [24] P. Zhang, M. Liguori, R. Bean, and S. Dodelson, *Phys. Rev. Lett.* **99**, 141302 (2007)
- [25] J. Dunkley et al. (WMAP), *Astrophys. J. Suppl. Ser.* **180**, 306 (2009)
- [26] H. Oyaizu, M. Lima, and W. Hu, *Phys. Rev. D* **78**, 123524 (2008)
- [27] R. Smith et al. (VIRGO), *Mon. Not. R. Astron. Soc.* **341**, 1311 (2003)
- [28] M. Takada and B. Jain, *Mon. Not. R. Astron. Soc.* **348**, 897 (2004)
- [29] V. F. Mukhanov, H. A. Feldman, and R. H. Brandenberger, *Phys. Rep.* **215**, 203 (1992)
- [30] S. M. Carroll, *Spacetime and Geometry* (Pearson Education, 2004)
- [31] M. Bartelmann, P. Schneider, *Phys. Rep.* **340**, 291 (2001)
- [32] M. A. Amin, R. V. Wagoner, and R. D. Blandford, *Mon. Not. R. Astron. Soc.* **390**, 131 (2008)
- [33] Y.-S. Song and K. Koyama, *J. Cosmol. Astropart. Phys.* **1**, 48 (2009)
- [34] Y.-S. Song and O. Doré, *J. Cosmol. Astropart. Phys.* **3**, 25 (2009)
- [35] M. White and Y.-S. Song, arXiv:0810.1518
- [36] V. Acquaviva, A. Hajian, D. N. Spergel, and S. Das, *Phys. Rev. D* **78**, 043514 (2008)
- [37] G.-B. Zhao, L. Pogosian, A. Silvestri, and J. Zylberberg, *Phys. Rev. D* **79**, 003513 (2009)
- [38] G.-B. Zhao, L. Pogosian, A. Silvestri, and J. Zylberberg, arXiv:0905.1326
- [39] F. Schmidt, *Phys. Rev. D* **78**, 043002 (2008)
- [40] F. Schmidt, arXiv:0905.0858
- [41] J. Khoury and M. Wyman, arXiv:0903.1292
- [42] A. Albrecht et al. (DETF), astro-ph/0609591
- [43] M. S. Vogeley and A. Szalay, *Astrophys. J.* **465**, 34 (1996)
- [44] M. Tegmark, A. N. Taylor, and A. F. Heavens, *Astrophys. J.* **480**, 22 (1997)
- [45] M. Takada and B. Jain, *Mon. Not. R. Astron. Soc.* **395**, 2065 (2009)
- [46] P. McDonald and U. Seljak, arXiv:0810.0323
- [47] T. Matsubara, *Astrophys. J.* **535**, 1 (2000)
- [48] <http://www.darkenergysurvey.org>

- [49] <http://www.lsst.org>
- [50] <http://jdem.gsfc.nasa.gov>
- [51] <http://cosmology.lbl.gov/BOSS>
- [52] R. Scoccimarro, Phys. Rev. D **70**, 083007 (2004)
- [53] W. Hu, Astrophys. J. Lett. **522**, L21 (1999)
- [54] D. N. Limber, Astrophys. J. **117**, 134 (1953)
- [55] N. Kaiser, Mon. Not. R. Astron. Soc. **227**, 1 (1987)
- [56] A. J. S. Hamilton, in *The Evolving Universe*, Astrophysics and Space Science Library Series **231**, 185 (1998)
- [57] M. Tegmark et al. (SDSS), Astrophys. J. **606**, 702 (2004)
- [58] F. Bernardeau, S. Colombi, E. Gaztañaga, and R. Scoccimarro, Phys. Rep. **367**, 1 (2002)
- [59] M. Tegmark and A. J. S. Hamilton, Mon. Not. R. Astron. Soc. **335**, 887 (2002)
- [60] J. R. Shaw and A. Lewis, Phys. Rev. D **78**, 103512 (2008)
- [61] H. A. Feldman, N. Kaiser, and J. A. Peacock, Astrophys. J. **426**, 23 (1994)
- [62] Y.-S. Song, I. Sawicki, W. Hu, Phys. Rev. D **75**, 064003 (2007)